

Observation of magnetoelectric effect in epitaxial ferroelectric film/manganite crystal heterostructures

T. Wu,^{1,2} M. A. Zurbuchen,^{1,2} S. Saha,¹ R.-V. Wang,^{1,2} S. K. Streiffer,^{1,2} and J. F. Mitchell¹

¹Material Science Division, Argonne National Laboratory, 9700 S. Cass Avenue, Argonne, Illinois 60439, USA

²Center for Nanoscale Materials, Argonne National Laboratory, 9700 S. Cass Avenue, Argonne, Illinois 60439, USA

(Received 29 September 2005; revised manuscript received 15 February 2006; published 17 April 2006)

A multiferroic heterostructure is constructed by growing an epitaxial piezoelectric $\text{Pb}(\text{Zr}_{0.3}\text{Ti}_{0.7})\text{O}_3$ film on a magnetostrictive layered manganite single crystal of composition $\text{La}_{1.2}\text{Sr}_{1.8}\text{Mn}_2\text{O}_7$. The efficient mechanical coupling at the interface results in a remarkable magnetoelectric (ME) effect. The ME voltage is $\sim 87\%$ of the theoretical value predicted by a phenomenological thermodynamic model. The ME effect peaks at the ferro-magnetic transition temperature of the manganite, a consequence of its magnetostrictive characteristics.

DOI: [10.1103/PhysRevB.73.134416](https://doi.org/10.1103/PhysRevB.73.134416)

PACS number(s): 75.80.+q, 75.47.Lx, 75.47.Gk, 77.55.+f

I. INTRODUCTION

Multiferroics are materials or structures where different ferroic orders such as (anti)ferroelectrics, (anti)ferromagnetics, and ferroelastics coexist.¹ In multiferroic magnetoelectrics, a dielectric polarization can be induced by an external magnetic field or conversely, a magnetic moment can be induced by an external electric field, a phenomenon known as the magnetoelectric (ME) effect.^{2,3} The physics inherent in this class of multiferroics has received much recent attention, as the mechanisms by which the different order parameters can be coupled are generally poorly understood, and as the cooperative interactions driving the different ferroic behaviors are often thought to arise from potentially incompatible electronic structures. The intensive research efforts have also been motivated by the large ME effect potentially achievable in these compounds. Materials systems with a strong ME effect at room temperature have potential applications as data storage and switching devices, actuators, transducers, magnetic field and stress sensors, and devices in optoelectronics and microwave electronics.^{3,4}

Examples of single-phase multiferroic materials are TbMnO_3 , TbMn_2O_5 , BiFeO_3 , BiMnO_3 , and some hexagonal manganites $R\text{MnO}_3$ with rare earth elements $R \in \{\text{Sc}, \text{Y}, \text{In}, \text{Ho} - \text{Lu}\}$.⁵⁻¹⁰ One main reason for the scarcity of multiferroics is that the ligand-field hybridization of a transition metal cation by its surrounding anions, which is often responsible for conventional ferroelectricity, requires that the d orbitals of the cations are unoccupied, therefore precluding ferromagnetism.^{11,12} Even the single-phase multiferroics listed above often exhibit only weak magnetization and/or ferroelectricity, and the relevant phase transitions from which magnetoelectric behavior is derived are often well below room temperature. A strong ME effect at room temperature, however, can be realized in a two-phase or multiphase composite in which the mechanical deformation of the magnetostrictive phase results in polarization in the piezoelectric phase.¹³⁻¹⁵ Bilayers and multilayers of such composites are especially promising due to their low leakage current and superior poling properties.¹⁶⁻¹⁹ Typical fabrication procedures involve tape-casting and sintering together thick (hundreds of micrometers) polycrystalline films.¹⁷

However, such an approach often suffers from several shortcomings: (1) poor mechanical coupling between layers due to the nonepitaxial nature of the interface; (2) impurities as a result of interfacial diffusion or reaction under high sintering temperatures; (3) lack of scaling capabilities. On the other hand, even with an epitaxial and coherent interface, epitaxial multilayers of thin films often yield a negligible ME effect due to substrate clamping.²⁰ Given these difficulties, an unambiguous description of the ME effect based on the underlying mean-field behavior of the constituents of the composites has still not been achieved.

Therefore it is desirable to construct multiferroic structures using a carefully selected substrate that is magnetically and elastically functional by itself. Then a ferroelectric film can be epitaxially grown on the substrate, which results in a heterostructure with an efficient in-plane elastic coupling. Such a substrate must satisfy several conditions: (1) a giant anisotropic magnetostriction;²¹ (2) good in-plane lattice match to the ferroelectric film; (3) reasonably good conductivity that eliminates the need for a separate electrode at the interface.

A very attractive materials family that may meet these criteria is the naturally layered manganites. Mixed-valent ($\text{Mn}^{3+}\text{-Mn}^{4+}$) manganites have captured much attention in condensed matter science recently due to their exotic electronic and magnetic properties, including complex insulator-metal transitions and colossal magnetoresistance.²² In some mixed-valent manganites, the strong coupling between magnetic field and lattice results in giant anisotropic magnetostriction, especially if the structural transition temperature (T_S) is close to the ferromagnetic ordering temperature (T_C).²³ It is important to note that unlike in conventional ferromagnets, the giant magnetostriction in layered manganites is a result of a field-induced change in the orbital-state occupancy.²¹

In the current study, we focus on the $n=2$ member of the Ruddlesden-Popper series of layered manganites $\text{La}_{2-2x}\text{Sr}_{1+2x}\text{Mn}_2\text{O}_7$ (LSMO) with $x=0.4$.^{24,25} Besides satisfying the conditions listed above, these layered manganites are easy to cleave along the a - b plane to achieve atomically flat surface areas of hundreds of square micrometers. We select $\text{Pb}(\text{Zr}_{0.3}\text{Ti}_{0.7})\text{O}_3$ (PZT), tetragonal at room temperature, as

the ferroelectric film based on the facts that it is a well-studied material with a large polarization and is both chemically and structurally compatible with LSMO.

Here we report our study on a unique heterostructure composed of a PZT layer epitaxially deposited on a layered manganite crystal of composition $\text{La}_{1.2}\text{Sr}_{1.8}\text{Mn}_2\text{O}_7$. While not optimal from an applications standpoint because of the relatively low T_C of the manganite constituent, this combination has many advantages as a model system. In this multiferroic structure, the manganite crystal serves as the substrate for the PZT film growth, as the magnetostrictive element and as the bottom electrode in the device. Without the constraint from conventional substrates, such a geometry maximizes the efficiency of in-plane transfer of the magnetostrictive strain from LSMO to the PZT film, and as we will describe below is amenable to a straightforward modeling of the ME effect. Indeed we find a strong strain-mediated coupling between the ferromagnet and the ferroelectric due to the epitaxial nature of the interface and the absence of substrate clamping. In a related study on similar heterostructures, we observed an abrupt change of polarization in the PZT film at the ferromagnetic transition temperature (T_C) of a LSMO crystal.²⁶ This modulation of polarization originates from the contraction of the in-plane lattice parameters of LSMO at T_C . In the current paper, a large ME effect is observed at T_C of LSMO where it exhibits the highest magnetostrictive sensitivity to an applied magnetic field. A model based on the phenomenological mean-field description of the ferroelectric PZT is shown to successfully describe the ME voltage that is generated by applied magnetic field.

II. EXPERIMENTAL PROCEDURES

Crystals of $\text{La}_{1.2}\text{Sr}_{1.8}\text{Mn}_2\text{O}_7$ were melt grown in flowing 20% O_2 (balance Ar) using a floating zone optical image furnace (NEC model SC-M15HD) as described previously.²⁷ The resulting boule cleaves readily to yield shiny black crystals. Energy-dispersive spectroscopy (Oxford Instruments Link Isis) indicates that the metal stoichiometry is equal to the nominal composition within experimental error. Tetragonal PZT films with a ratio of Zr:Ti=30:70 were deposited by chemical solution deposition (CSD) on cleaved manganite crystals. We also fabricated samples by depositing PZT films on polished manganite crystals, yielding equivalent results. CSD methods including both sol-gel and metallo-organic decomposition have been routinely used to prepare PZT films with properties comparable to those of single crystals.²⁸ The details of the film deposition and solution chemistry used for our sample preparation have been reported elsewhere.²⁹ Specifically, an alkoxide precursor solution with 10% lead excess was spin coated onto the freshly prepared manganite surface. The final film thickness is ~ 1100 Å after annealing at 650 °C for 20 min in air (only one coating was required to achieve the desired thickness). Platinum top electrodes with areas between 7.85×10^{-5} and 1.96×10^{-3} cm^2 were deposited at ~ 200 °C by electron beam evaporation through a shadow mask to define discrete capacitors. After top electrode deposition, the samples were heated again at ~ 550 °C for 10 min in flowing oxygen to optimize the ferroelectric/top electrode interface.

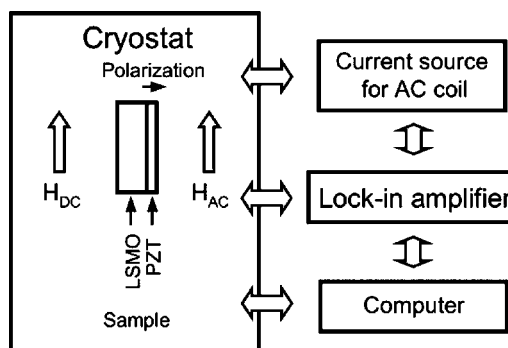


FIG. 1. Experimental setup for the ME measurement.

Structural characterization was carried out using a Philips X'pert MRD system. The dielectric properties of the PZT film were studied using an HP4192A impedance analyzer and a Radiant Technologies RT6000 ferroelectric test system. The magnetization of the manganite crystal was measured in a Quantum Design physical properties measurement system (PPMS). Figure 1 shows a block diagram of the experimental setup for the ME characterization. The sample was measured at selected temperatures in the PPMS cryogenic chamber which provides a static magnetic field H_{dc} parallel to the sample surface. An ac field H_{ac} ($H_{ac}=0.1-10$ Oe at 100 Hz–10 kHz) along the same direction was generated by a coil concentric with the primary dc superconducting magnet. The induced ME voltage across the sample, V_{ME} , was measured using a lock-in technique. Our setup corresponds to a transverse geometry, which often results in a stronger effect than the longitudinal geometry where all H_{dc} , H_{ac} , and V_{ME} are perpendicular to the sample plane.¹⁸ For each temperature, to minimize the effect of magnetic hysteresis, the sample was heated to room temperature first before cooling down to the specific temperature in the presence of a poling voltage of +6 V to the top electrode.

III. EXPERIMENTAL RESULTS

Figure 2(a) is an x-ray θ - 2θ scan of the sample. The layered manganite crystal has a tetragonal structure with $a = 3.87$ Å and $c = 20.12$ Å at room temperature. For the PZT film, only the (00 l) reflections are detected and there are no visible secondary phases. The in-plane epitaxial relationship between the PZT film and the LSMO crystal was examined by an x-ray ϕ scan of (101)-type reflections as shown in Fig. 2(b) and confirmed to be PZT(001)//LSMO(001) and PZT(100)//LSMO(100) with fourfold symmetry. The FWHM are 0.89° and 0.08° for the PZT film and LSMO crystal, respectively.

The dielectric permittivity and the loss tangent vs electric field in Figs. 3(a) and 3(b), respectively, show little voltage shift and further confirm the good quality of the interface with a low density of charge traps between the PZT film and the LSMO crystal. The detailed measurement of polarization hysteresis and its temperature dependence are reported elsewhere.²⁶ The remanent polarization P_r at room temperature is ~ 44 $\mu\text{C}/\text{cm}^2$.

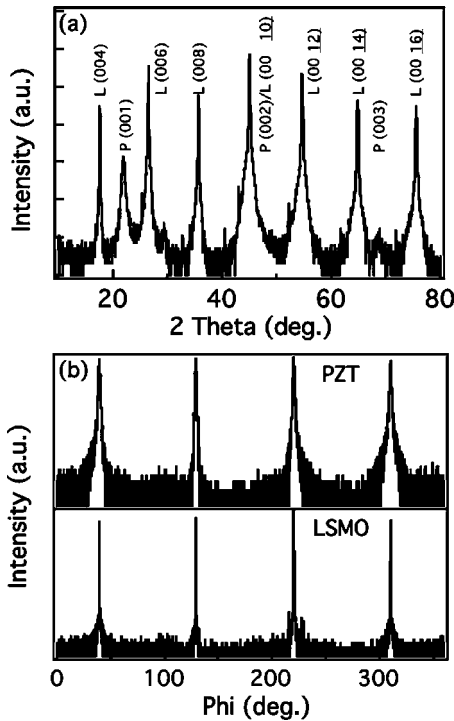


FIG. 2. (a) X-ray θ - 2θ scan and (b) ϕ scan for the 1100 Å PZT film deposited on a layered manganite crystal. In (a), diffraction peaks of the PZT film and the LSMO crystal are labeled as P and L, respectively. Both graphs are on logarithmic scales.

Figure 4 shows the static magnetic field dependence of the induced ME voltage at three temperatures: 50, 120, and 300 K.³⁰ All data were taken with $H_{ac}=2$ Oe and $f=1$ kHz. This frequency is below anticipated magnetoelctromechanical resonances for this particular geometry, and indeed no clear evidence for resonancelike frequency dependence was

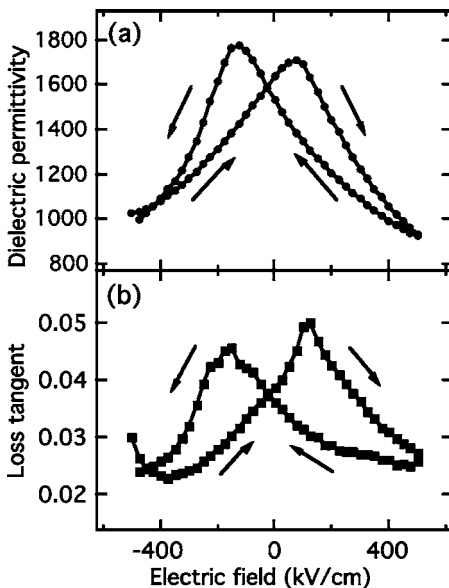


FIG. 3. (a) Dielectric permittivity and (b) loss tangent vs electric field measured on the PZT/LSMO heterostructure at room temperature. The arrows illustrate the directions of the voltage scans.

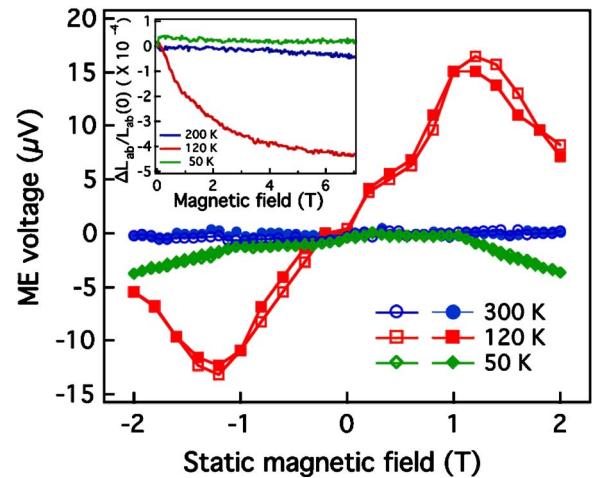


FIG. 4. (Color online) ME voltage vs static magnetic field measured with a transverse geometry at three different temperatures of 50, 120, and 300 K. The ME voltage is induced by an oscillating magnetic field H_{ac} with a magnitude of 2 Oe and a frequency of 1 kHz. The open (filled) symbols are the data taken with increasing (decreasing) H . The largest peak-to-peak ME voltage swing is $\sim 28 \mu\text{V}$, occurring at 120 K. The inset is the in-plane magnetostriction $[\Delta L_{ab}(H)/L_{ab}(0)]$ as a function of H measured at selected temperatures, taken from Ref. 23.

observed for the range of frequencies that is accessible with our measurement system. It is important to emphasize as well that our geometry is a rather different device configuration compared to the many-micrometer layer thicknesses of the laminate composites that are commonly studied.³¹ The strongest ME effect is at 120 K, near T_C of the manganite crystal. As H_{dc} is ramped up from zero, V_{ME} first increases, then peaks at ~ 1 T with a magnitude of $\Delta V_{ME} \sim 15 \mu\text{V}$, and finally decreases at higher field. V_{ME} goes through zero as H_{dc} ramps down and switches its direction, accompanied by a 180° shift in V_{ME} . Similar features have been observed in layered composite of thick films made by tape casting.¹⁷ At 120 K, the peak-to-peak difference of the ME voltage swing is $\sim 2\Delta V_{ME}$ or 28 μV .

This ME effect is much weaker at 50 K and room temperature, away from T_C . This strong temperature dependence is a result of the magnetostrictive properties of the manganite crystal, as demonstrated by the data of Kimura *et al.*, shown in the inset of Fig. 4.²¹ As the temperature approaches T_C , magnetostriction along both the ab plane and the c axis increase in accordance with the enhancement of the magneto-resistance effect. At 120 K, the in-plane lattice contraction $\Delta L_{ab}/L_{ab}(0)$, or equivalently λ , reaches a value of 4.4×10^{-4} under a magnetic field of 7 T, which is comparable to that of the best magnetostrictive materials such as the TbDyFe₂ alloy (Terfenol-D).³² However, the magnetostriction of the manganite crystal is much smaller at lower fields (only $\sim 100 \times 10^{-6}$ under 5000 Oe, compared to 1600×10^{-6} for Terfenol-D under the same field). The temperature dependence of the striction without magnetic field also shows a contraction of the in-plane lattice plane of $\sim 0.1\%$ at T_C , more evidence of the structural instability at this temperature. In Fig. 5, we plot together the temperature depen-

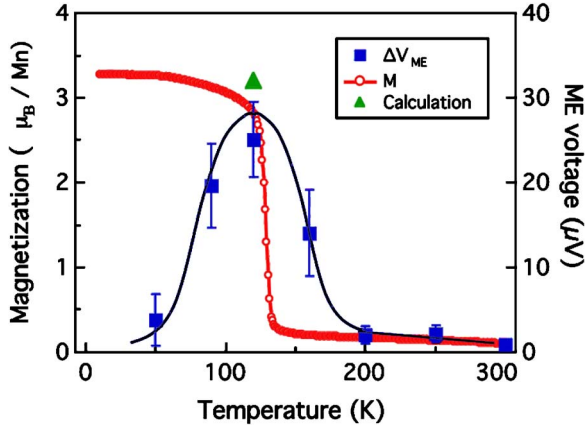


FIG. 5. (Color online) The comparison of the temperature dependence of the magnetization measured on the manganite crystal and the peak-to-peak ME voltages as shown in Fig. 3. The triangle is the theoretical calculated value for the ME voltage at 120 K based on the bulk data as outlined in the text. The continuous line is a guide to the eye.

dence of the peak-to-peak ME voltage and the dc magnetization of the manganite crystal measured with a magnetic field of 1000 Oe. The error bar on the ME voltage is the standard deviation of three different samples.

IV. DISCUSSION

We now compare our experimental results to the predictions of a phenomenological Landau-Ginzburg-Devonshire (LGD) theory describing thin ferroelectric films epitaxially grown on cubic substrates.^{33,34} For simplicity, we take cubic symmetry and define an orthogonal right-hand coordinate system with the three axis in the film surface normal direction. The in-plane polarizations P_1 and P_2 are taken both equal to zero, equivalent to the assumption of a ferroelectric transition to a tetragonal domain structure with out-of-plane polarization only. This is justified given the polarization hysteresis loops, and by the fact that for tetragonal PZT films, any domains with in-plane polarization are generally very difficult to reorient. Then the general expression for the thermodynamic potential \tilde{G} of a thin ferroelectric film on a thick substrate is the Legendre transformation of the standard elastic Gibbs function³⁴

$$\tilde{G} = \alpha_3^* P_3^2 + \alpha_{33}^* P_3^4 + \alpha_{111} P_3^6 + \frac{u_m^2}{s_{11} + s_{12}},$$

TABLE I. Values of coefficients used for the renormalized thermodynamic potential in Eq. (1). All data were taken on bulk samples of PZT with Zr:Ti=30:70 except the elastic compliances, which were measured on PbTiO₃ (Refs. 34 and 37–39).

T_C (°C)	C (10^5 °C)	Q_{12} (10^{-2} m ⁴ /C ²)	α_{11} (10^7 m ⁵ /C ² F)	α_{111} (10^8 m ⁹ /C ⁴ F)	s_{11} (m ² /N)	s_{12} (m ² /N)
440.2	1.881	-2.480	0.6458	2.348	8.0×10^{-12}	-2.5×10^{-12}

$$\alpha_3^* = \frac{T - \theta}{2\varepsilon_0 C} - u_m \frac{2Q_{12}}{s_{11} + s_{12}}, \quad \alpha_{33}^* = \alpha_{11} + \frac{Q_{12}^2}{s_{11} + s_{12}}, \quad (1)$$

where $\alpha_i, \alpha_{ij}, \alpha_{ijk}$ are ferroelectric dielectric stiffnesses at constant stress; s_{ij} are the elastic compliances at constant polarization; Q_{ij} is the electrostrictive coupling between the ferroelectric polarization and stress; θ is the Curie-Weiss temperature; ε_0 is the permittivity of free space; C is the Curie-Weiss constant; and u_m is the misfit strain. The mechanical two-dimensional clamping breaks the symmetry of the system and renormalizes the second- and fourth-order polarization terms. We note that the phenomenological treatment given here does not consider the effect of the depolarizing field or the detailed domain configurations.^{35,36} The relations among polarization, strain, and temperature can be achieved by minimizing this thermodynamic potential using the appropriate dielectric stiffnesses α :

$$\frac{1}{P_3} \frac{\partial \tilde{G}}{\partial P_3} = 2\alpha_3^* + 4\alpha_{33}^* P_3^2 + 6\alpha_{111} P_3^4 = 0. \quad (2)$$

Solving Eq. (2), we can write P_3 as a function of u_m , the misfit strain:

$$\begin{aligned} P_3 &= \left(\frac{-\alpha_{33}^* + (\alpha_{33}^{*2} - 3\alpha_{111}\alpha_3^*)^{1/2}}{3\alpha_{111}} \right)^{1/2} \\ &= \left(\frac{1}{3\alpha_{111}} \right)^{1/2} \left\{ \left[\left(\alpha_{11} + \frac{Q_{12}^2}{s_{11} + s_{12}} \right)^2 \right. \right. \\ &\quad \left. \left. - 3\alpha_{111} \left(\frac{T - \theta}{2\varepsilon_0 C} - u_m \frac{2Q_{12}}{s_{11} + s_{12}} \right) \right] \right. \\ &\quad \left. - \left(\alpha_{11} + \frac{Q_{12}^2}{s_{11} + s_{12}} \right) \right\}^{1/2}. \end{aligned} \quad (3)$$

The values of the LGD coefficients in \tilde{G} used in this calculation were measured by Haun *et al.* on bulk samples and are listed in Table I.^{37–39} The calculated polarization of the PZT film as a function of the misfit strain u_m is shown in Fig. 6. The polarization decreases (increases) with tensile (compressive) strain. This trend is qualitatively consistent with the experimental results obtained by Kumazawa *et al.* using a mechanical bending instrument.⁴⁰ Also shown in Fig. 6 is the percent change of the polarization, $\Delta P/P$, when the misfit strain is modulated by 0.1%, which is essentially the derivative of the P vs u_m curve. This strain-induced modulation of P is as large as a few percent and is a sensitive function of the strain state in the film.

In the formulation of Pertsev, Zembilgotov, and Tagantsev,³⁴ symmetry breaking is represented in the misfit

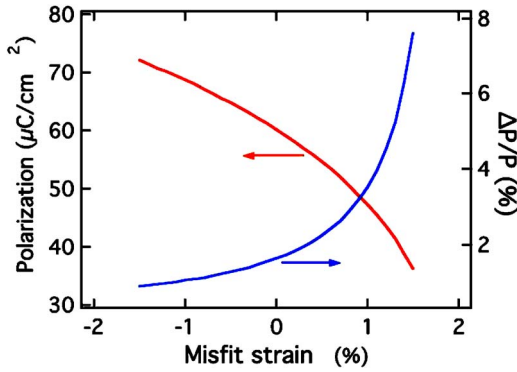


FIG. 6. (Color online) Polarization of the PZT film as a function of the misfit strain calculated using the phenomenological Landau-Ginzburg-Devonshire theory. Also shown is the percent change in polarization as the misfit strain is modulated by 0.1%.

strain u_m . In the PZT/LSMO structure, if we only consider the substrate/film lattice mismatch at room temperature relative to the extrapolated pseudocubic lattice parameter of the PZT as is relevant for LGD calculations,³⁸ there is a compressive strain $(3.87-4.02 \text{ \AA})/3.87 \text{ \AA} = -3.9\%$. However, as Speck and Pompe pointed out,³⁶ the effective misfit strain associated with a film grown on a substrate after some amount of relaxation is controlled by an effective substrate lattice parameter b^* :

$$b^* = b(T)(1 - \rho_i b_{edge,i}) \quad (4)$$

where b is the substrate lattice parameter and $\rho_i b_{edge,i}$ (i is either 0, 1, or 2) is the strain relief provided by the misfit dislocations at the film/substrate interface. In other words, b and u_m must be modified to account for the misfit dislocations and relaxation associated with the film growth.

Although it is difficult to evaluate an accurate value of u_m given the film growth process and the complicated electro-mechanical conditions, we can assume that u_m is close to zero. In the CSD process there are several sources that contribute to the residual biaxial stresses built up in the film: the most relevant ones are the intrinsic stress σ_{int} and the thermal stress σ_{th} .⁴¹⁻⁴³ The magnitude of the intrinsic stress is largely determined by the film deposition conditions, i.e., spin speed, viscosity of sol, humidity, etc. After spin coating, a tensile stress always exists in an as-spun film due to evaporation of water and solvent at low temperatures. During subsequent heating, organic decomposition and pyrolysis of nonvolatile species result in additional stress development. The thermal stress dominates during the process of cooling from the annealing temperature (650 °C in our case), which originates from the temperature-dependent lattice mismatch between the film and the substrate.⁴¹ At the same time, strain relaxation can occur through the formation of mixed ferroelectric domains and interfacial misfit dislocations at the film/substrate interface. As a starting point, we assume that the residual strain after the film growth process is close to zero, as these films are thick enough to be at least partially relaxed by dislocation formation and twinning.

The ME effect of the system can be treated as a special case of “product properties” of composite materials,¹³ in

which the overall response coefficient $\alpha = \partial Z / \partial X$ is determined by the product of the individual responses, $\partial Y / \partial X|_1 \times \partial Z / \partial Y|_2$. In other words, the ME voltage occurs as a result of the product property between the individual magnetostrictive and piezoelectric responses:

$$\frac{\Delta V}{\Delta H} = \frac{1}{C_0} \left(\frac{\partial P}{\partial u_m} \right)_{PZT} \left(\frac{\partial u_m}{\partial H} \right)_{LSMO} \quad (5)$$

where C_0 is the capacitance per unit area of the heterostructure. Combining Eqs. (3) and (5) and the magnetostriction data in the inset of Fig. 4, we estimate the maximum of $\Delta V_{ME} \sim 16 \mu\text{V}$ with ΔH of 2 Oe. Then the modulation of V_{ME} by a static magnetic field is $2\Delta V_{ME}$, or $32 \mu\text{V}$, which agrees reasonably well with the experimental value of $28 \mu\text{V}$. Besides the intrinsic limitations of the phenomenological model as we discussed above, the major discrepancy between theoretical and experimental results comes from the fact that all the thermodynamic coefficients of PZT are measured on bulk crystals, not thin films.³⁷⁻³⁹ In particular, elastic properties of CSD thin films may differ considerably from bulk. Furthermore, it was proposed that the stress state upon cooling through the Curie temperature can influence the domain configuration, and thus dielectric properties, in tetragonal PZT thin films.⁴⁴ A compressive stress on cooling from the cubic state causes a majority of domains aligned normal to the film plane (type- c orientation), whereas a tensile stress results in in-plane polar direction (type- a orientation). In our case, the lower remnant polarization P_r than the bulk value implies that some fraction of ferroelectric domains are in plane and do not yield a switchable polarization along the direction of the applied electric field, commensurately reducing the tunability of polarization and V_{ME} .

Comparison between the theoretical prediction and the experimental data allows us to conclude that the ME effect observed here is intrinsic for this PZT/LSMO system. Further, the close agreement between theory and experiment within the limits of the assumptions that must be made indicates that, as expected, reorientation of a -axis domains (which would greatly enhance the ME effect) is not significant for our heterostructures containing thin planar PZT layers. In our system, the stress transfer across the interface between the LSMO crystal and the PZT film is quite effective. On the contrary, among the laminated structures composed of polycrystalline thick layers, PZT/LSMO shows the weakest ME voltage coefficient with the measured value being an order of magnitude smaller than the estimates.¹⁸ The same trend was observed in bilayers of lead magnesium niobate-lead titanate and yttrium iron garnet (YIG).⁴⁵ The ME interaction is dramatically strengthened in samples with epitaxial YIG films and is the weakest in samples with polycrystalline YIG.

V. CONCLUSIONS

In conclusion, we have demonstrated a ME effect in a multiferroic heterostructure composed of a PZT thin film epitaxially deposited on a layered manganite crystal. Assuming a near-zero strain state and using the bulk LGD coefficients, we found that the experimentally observed ME voltage is

~87% of the theoretical value estimated from a phenomenological thermodynamic model. Limited only by the thickness of the PZT film, the ME voltage coefficient in our approach could be as high as 600 mV/cm Oe, which is comparable to the highest values obtained in the laminate composites.^{15,18,46–48} Further enhancement of the ME effect could be achieved by carefully adjusting the measurement geometry and frequency of the ac magnetic field. Another straightforward way of optimizing the ME effect is by selecting materials with a larger piezoelectric coefficient such as Pb(Mg_{1/3}Nb_{2/3})O₃-PbTiO₃.⁴⁹ Finally, patterning the piezoelectric thin films into discrete submicrometer islands could

also increase the ME response since it facilitates the movement of ferroelectric domain walls and recovers the properties of single-domain crystals.⁵⁰

ACKNOWLEDGMENTS

Work at Argonne National Laboratory is supported by the U.S. Department of Energy, Office of Science, Office of Basic Energy Sciences, under Contract No. W-31-109-ENG-38. We are grateful to T. Kimura for providing the magnetostriction data on the bilayer LSMO crystals.

- ¹L. D. Landau and E. M. Lifshitz, *Electrodynamics of Continuous Media* (Pergamon, Oxford, 1960), p. 119.
- ²H. Schmid, *Ferroelectrics* **162**, 317 (1994).
- ³M. Fiebig, *J. Phys. D* **38**, R123 (2005).
- ⁴V. E. Wood and A. E. Austin, *Int. J. Magn.* **5**, 303 (1973).
- ⁵T. Kimura, T. Goto, H. Shintani, K. Ishizaka, T. Arima, and Y. Tokura, *Nature (London)* **426**, 55 (2003).
- ⁶N. Hur, S. Park, P. A. Sharma, J. S. Ahn, S. Guha, and S-W. Cheong, *Nature (London)* **429**, 392 (2004).
- ⁷J. Wang, J. B. Neaton, H. Zheng, V. Nagarajan, S. B. Ogale, B. Liu, D. Viehland, V. Vaithyanathan, D. G. Schlom, U. V. Waghmare, N. A. Spaldin, K. M. Rabe, M. Wuttig, and R. Ramesh, *Science* **299**, 1719 (2003).
- ⁸T. Kimura, S. Kawamoto, I. Yamada, M. Azuma, M. Takano, and Y. Tokura, *Phys. Rev. B* **67**, 180401(R) (2003).
- ⁹A. V. Kovalev and G. T. Andreeva, *C. R. Hebd. Seances Acad. Sci.* **256**, 1958 (1963).
- ¹⁰M. Fiebig, Th. Lottermoser, D. Fröhlich, A. V. Goltsev, and R. V. Pisarev, *Nature (London)* **419**, 818 (2002).
- ¹¹R. E. Cohen, *Nature (London)* **358**, 136 (1992).
- ¹²N. A. Hill, *J. Phys. Chem. B* **104**, 6694 (2000).
- ¹³J. van Suchtelen, *Philips Res. Rep.* **27**, 28 (1972).
- ¹⁴C. W. Nan, *Phys. Rev. B* **50**, 6082 (1994).
- ¹⁵J. Ryu, S. Priya, A. V. Carazo, K. Uchino, and H. E. Kim, *J. Am. Ceram. Soc.* **84**, 2905 (2001).
- ¹⁶G. Harshe, Ph.D. thesis, Pennsylvania State University, 1991.
- ¹⁷G. Srinivasan, E. T. Rasmussen, B. Levin, and R. Hayes, *Phys. Rev. B* **65**, 134402 (2002).
- ¹⁸M. I. Bichurin, V. M. Petrov, and G. Srinivasan, *Phys. Rev. B* **68**, 054402 (2003).
- ¹⁹S. Dong, J. F. Li, and D. Viehland, *Appl. Phys. Lett.* **83**, 2265 (2003).
- ²⁰K. Lefki and G. J. M. Dormans, *J. Appl. Phys.* **76**, 1764 (1994).
- ²¹T. Kimura, Y. Tomioka, A. Asamitsu, and Y. Tokura, *Phys. Rev. Lett.* **81**, 5920 (1998).
- ²²A. P. Ramirez, *J. Phys.: Condens. Matter* **9**, 8171 (1997).
- ²³A. Asamitsu, Y. Moritomo, Y. Tomioka, T. Arima, and Y. Tokura, *Nature (London)* **373**, 407 (1995).
- ²⁴A. Asamitsu, Y. Moritomo, H. Kuwahara, and Y. Tokura, *Nature (London)* **380**, 141 (1996).
- ²⁵J. F. Mitchell, D. N. Argyriou, A. Berger, K. E. Gray, R. Osborn, and U. Welp, *J. Phys. Chem. B* **105**, 10731 (2001).
- ²⁶M. A. Zurbuchen, T. Wu, S. Saha, J. F. Mitchell, and S. K. Streiffer, *Appl. Phys. Lett.* **87**, 232908 (2005).
- ²⁷J. F. Mitchell, D. N. Argyriou, J. D. Jorgensen, D. G. Hinks, C. D. Potter, and S. D. Bader, *Phys. Rev. B* **55**, 63 (1997).
- ²⁸Robert W. Schwartz, *Chem. Mater.* **9**, 2325 (1997).
- ²⁹D.-J. Kim, D. Y. Kaufman, S. K. Streiffer, T. H. Lee, R. Erck, and O. Auciello, in *Ferroelectric Thin Films XI*, MRS Symposia Proceedings No. 748 (Materials Research Society, Pittsburgh, 2003), U15.4.1.
- ³⁰We subtracted from the experimental data the parasitic voltage signals associated with the instrument setup. These signals have no magnetic field dependence and their magnitudes are not reproducible.
- ³¹S. Dong, J. Cheng, J. F. Li, and D. Viehland, *Appl. Phys. Lett.* **83**, 4812 (2003).
- ³²A. B. Flatau, M. J. Dapino, and F. T. Calkins, in *Comprehensive Composite Materials* (Elsevier, Amsterdam, 2000), Vol. 5.
- ³³A. F. Devonshire, *Philos. Mag.* **740**, 1040 (1949).
- ³⁴N. A. Pertsev, A. G. Zembilgotov, and A. K. Tagantsev, *Phys. Rev. Lett.* **80**, 1988 (1998).
- ³⁵D. R. Tilley and B. Zeks, *Ferroelectrics* **134**, 313 (1992).
- ³⁶J. S. Speck and W. Pompe, *J. Appl. Phys.* **76**, 466 (1994).
- ³⁷M. J. Haun, E. Furman, S. J. Jang, and L. E. Cross, *Ferroelectrics* **99**, 13 (1989).
- ³⁸M. J. Haun, E. Furman, H. A. McKinstry, and L. E. Cross, *Ferroelectrics* **99**, 27 (1989).
- ³⁹M. J. Haun, Z. Q. Zhuang, E. Furman, S. J. Jang, and L. E. Cross, *Ferroelectrics* **99**, 45 (1989).
- ⁴⁰T. Kumazawa, Y. Kumagai, H. Miura, M. Kitano, and K. Kushida, *Appl. Phys. Lett.* **72**, 608 (1998).
- ⁴¹G. A. C. M. Spierings, G. J. M. Dormans, W. G. J. Moors, M. J. E. Ulenaers, and P. K. Larsen, *J. Appl. Phys.* **78**, 1926 (1995).
- ⁴²S. S. Sengupta, S. M. Park, D. A. Payne, and L. H. Allen, *J. Appl. Phys.* **83**, 2291 (1998).
- ⁴³R. J. Ong and D. A. Payne, *Br. Ceram. Trans.* **103**, 97 (2004).
- ⁴⁴G. L. Brennecke, W. Huebner, B. A. Tuttle, and P. G. Clem, *J. Am. Ceram. Soc.* **87**, 1459 (2004).
- ⁴⁵G. Srinivasan, C. P. De Vreugd, M. I. Bichurin, and V. M. Petrov, *Appl. Phys. Lett.* **86**, 222506 (2005).
- ⁴⁶Shuxiang Dong, Jie-Fang Li, and D. Viehland, *Appl. Phys. Lett.* **85**, 5305 (2004).
- ⁴⁷K. Mori and M. Wuttig, *Appl. Phys. Lett.* **81**, 100 (2002).
- ⁴⁸G. Srinivasan, E. T. Rasmussen, J. Gallegos, R. Srinivasan, Yu. I. Bokhan, and V. M. Laletin, *Phys. Rev. B* **64**, 214408 (2001).
- ⁴⁹L. Bellaiche and David Vanderbilt, *Phys. Rev. Lett.* **83**, 1347 (1999).
- ⁵⁰V. Nagarajan, A. Roytburd, A. Stanishevsky, S. Prasertchoung, T. Zhao, L. Chen, J. Melngailis, O. Auciello, and R. Ramesh, *Nat. Mater.* **2**, 43 (2003).